SPACE SCIENCES

High mobility of asteroid particles revealed by measured cohesive force of meteorite fragments

Yuuya Nagaashi†* and Akiko M. Nakamura

Copyright © 2023 The Authors, some rights reserved; exclusive licensee American Association for the Advancement of Science. No claim to original U.S. Government Works. Distributed under a Creative Commons Attribution NonCommercial License 4.0 (CC BY-NC).

The cohesive force of asteroid particles is a crucial parameter in microgravity. The cohesive force was evaluated under the assumptions of lunar regolith and proportionality to particle size; however, it is sensitive to particle shape. In this study, cohesive-force measurements of meteorite fragments and aggregates consisting of silica microspheres revealed that the cohesive force is independent of the sizes of the fragments and aggregates as well as of the fragment preparation methods. The cohesive forces of the asteroid particles were found to be orders of magnitude smaller than previously predicted, explaining the high mobility of asteroid surface particles identified by space exploration.

INTRODUCTION

Cohesive and adhesive forces between similar and different types of particles, respectively (hereinafter, we use "cohesive" even if "adhesive" is more appropriate), are key to understanding the initial stages of planetary formation, evolutionary processes of small airless bodies, and eolian processes on planetary bodies. The cohesive force substantially affects coagulation processes, from submicrometer-sized grains to kilometer-sized planetesimals (*1*), and may be the dominant force influencing particles on small bodies in a microgravity environment (*2*). The cohesive force affects the size at which particles become suitable for migration on the surface owing to pressure from the gas from a spacecraft or seismic wave accelerations from impacts (*3*). It also affects the porosity of the surface related to the impact cratering efficiency and thermal inertia (*4*), the sampling efficiency in exploration missions (*5*), and the deformation and failure modes of rubble-pile asteroids along with accelerated rotation (*6*, *7*). The cohesive force also affects the wind friction threshold speed for particle movement on planetary bodies (*8*, *9*).

In theoretical descriptions of forces, such as the van der Waals forces (*10*) and the pull-off force of the Johnson-Kendall-Roberts (*11*) and Derjaguin-Muller-Toporov theories (*12*) for two macroscopic spheres, the force is proportional to the particle size, which has been experimentally confirmed for micrometer-sized spheres (*13*). However, direct measurements of the cohesive force of irregularly shaped meteorite fragments and glass spheres tens of micrometers in size have shown that the cohesive force is orders of magnitude smaller than theoretical predictions owing to the particle shape and surface roughness (*14*).

Direct measurements (*14*) were conducted under ambient conditions using fragments produced by crushing meteorite pieces using a mortar and pestle. However, the cohesive force is expected to be affected by the measurement conditions and changed under heat or evacuation conditions (*15*, *16*). Moreover, the actual asteroid particles are formed by impact fragmentation (*17*) or thermal fatigue (*18*). The difference in the formation processes may result in asteroid particles with different shapes and cohesive forces.

The dependence of the cohesive force on the fragment size is experimentally unconstrained, and it remains difficult to estimate the cohesive force of the asteroid particles based on previous measurements. To address these issues, we directly measured the cohesive force of particles against smooth slides using the centrifugal method (*14*, *19*, *20*). The particles were Allende and Tagish Lake carbonaceous chondrite fragments (micrometers or tens of micrometers in size) produced by mortar and pestle or projectile impact or aggregates (tens of micrometers) consisting of submicrometer-sized silica spheres as samples with well-characterized surface structures. Measurements were also conducted under evacuated conditions or after heating to observe these effects.

RESULTS AND DISCUSSION

We evaluated the shapes of the meteorite fragments using optical microscopy and confocal laser scanning microscopy with spatial resolutions of micrometers and submicrometers, respectively. We found no substantial differences according to fragmentation method (tables S3 and S4). There was no significant difference in cohesive-force measurements among fragments of the same meteorite, even if different fragmentation methods were used, according to a Mann-Whitney *U* test ($P = 0.28$ and 0.47, Allende and Tagish Lake meteorites, respectively, values that are much larger than 0.05). However, the cohesive force of the Allende fragments was several times greater than that of the Tagish Lake fragments (Fig. 1A). Scanning electron microscope (SEM) images revealed fine structures on the surface of Tagish Lake fragments that would not have been detected at the resolution of the optical profilometry described above (fig. S1). These results suggest that the cohesive force is controlled by the surface structures at submicrometer or smaller scales, regardless of the fragmentation method. Furthermore, the measurements confirmed that after heating, the cohesive force increased by approximately three- to fourfold (fig. S6). Heating reduces the amount of adsorbed water molecules and increases the proportion of silanol groups on the surface (*21*); thus, hydrogen bonding

Department of Planetology, Kobe University, 1-1 Rokkodaicho, Nada-ku, Kobe 657-8501, Japan.
†Present address: Department of Earth Science, Tohoku University, 6-3 Aza-aoba, Aramaki, Aoba-ku, Sendai 980-8578, Japan.
*Corresponding author. Email: y.nagaashi@tohoku.ac.jp

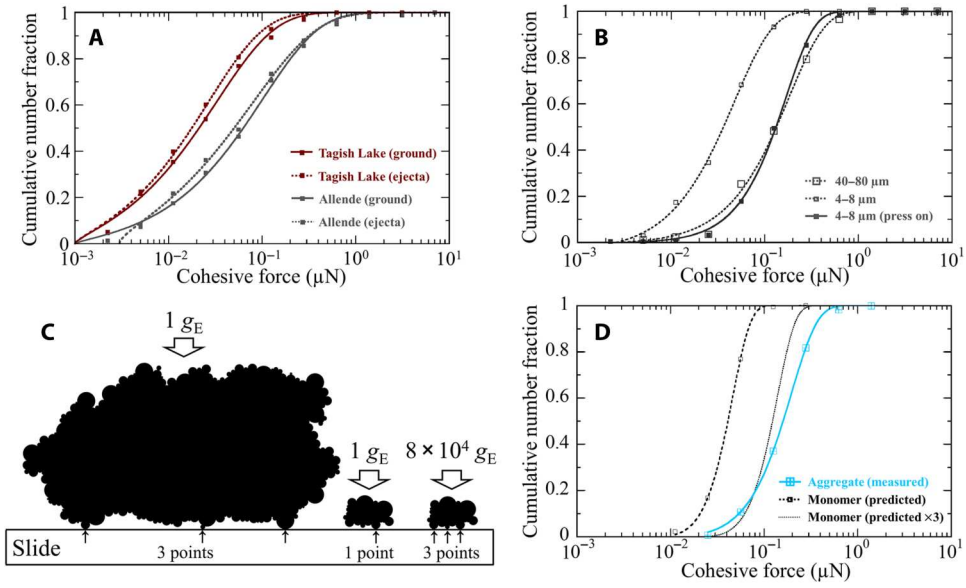

Fig. 1. Cohesive force of particles. (**A**) Measured cohesive force of Allende and Tagish Lake meteorite fragments, prepared by a mortar and pestle or projectile impact, against a smooth glass slide under ambient conditions. The fitted curves were obtained on the basis of Eq. 3; the fitting parameters are summarized in table S5. (**B**) Measured cohesive force of tens-of-micrometer– and micrometer-sized Allende fragments against a stainless steel slide under ambient conditions. The value of the large fragments is approximately twice greater than that against the glass slide in (A), which might be consistent with the trend that the Hamaker constant of metals is greater than that of silica (*10*). (**C**) Schematic diagram of the contact states of meteorite fragments of different sizes against slides inferred from the cohesive-force measurements. The left fragment represents tens-of-micrometer–sized fragments at 1 g_E, the middle fragment represents micrometer-sized fragments at 1 g_E, and the right fragment represents micrometer-sized fragments at 8 × 10^4 g_E. (**D**) Comparison of the measured cohesive force of aggregates tens of micrometers in size consisting of submicrometer-sized silica spheres against a glass slide under ambient conditions and the cohesive force estimated by the relationship obtained for the micrometer-sized silica spheres (*13*) based on the size distribution of the constituent spheres. Solid curve indicates measurements, dashed curve indicates predictions, and thin dotted curve indicates three times the prediction.

between the silanol groups may have been responsible for the greater cohesive force (*15*).

The measured cohesive force of the micrometer-sized meteorite fragments was approximately one-third that of the tens-of-micrometer–sized meteorite fragments. However, when we measured the cohesive force of the micrometer-sized fragments after pressing them against a slide at a centrifugal acceleration of approximately 8 × 10^4 g_E (where g_E is the acceleration of Earth's gravitational acceleration), the difference due to size differences was no longer significant (P = 0.94; Fig. 1B). It is unlikely that plastic deformation leading to an increased cohesive force (*20*) occurred during press-on (see Materials and Methods). We interpret this increase in cohesive force as the result of micrometer-sized particles contacting the slide at a single point under 1 g_E, whereas at 8 × 10^4 g_E, the particles contacted the slide at approximately three points, as occurs with particles tens of micrometers in size under 1 g_E (Fig. 1C) (*14*, *22*). This interpretation was supported by our aggregate measurements. The measured cohesive force of the tens-of-micrometer–sized aggregates was close to threefold that of the submicrometer-sized silica spheres that comprise the aggregates (Fig. 1D). This was estimated based on the relationship obtained for the micrometer-sized silica spheres (*13*). These results suggested that the cohesive forces of the meteorite fragments and aggregates were determined by their surface structures. Given that the cohesive force of silica aggregates could be expressed in terms of the size distribution of submicrometer-sized silica spheres and the empirical relationship between cohesive force and sphere diameter, it is possible that the cohesive force of the meteorite fragment also depends on the grains comprising the fragments, whether the grains are coarse or fine. Generally, meteorite constituent grains tend to be finer if they have experienced aqueous alteration, and coarser if they have experienced thermal alteration (*23*). Moreover, meteorites with a larger fraction of fine-grained matrix exhibited a weaker cohesive force. In comparison, meteorites with a larger fraction of molten grains (chondrules), or those that have undergone melting or severe thermal alteration (eucrite and petrologic type 6 chondrite), exhibit cohesive forces similar to those of terrestrial silica sand particles (Fig. 2), and the forces are larger compared to those of meteorite fragments with little or gentle thermal alteration (*14*). Thus, the cohesive force of meteorite fragments may be determined by whether the constituent grains are coarse or fine, reflects their evolutionary process, and is constant with respect to the fragment size (*14*) unless plastic deformation occurs (i.e., it is not proportional to the fragment size). Alternatively, a model based on a self-affine fractal surface down to the nanoscale showed that cohesive force was independent of particle size (*22*); however, the spatial resolution of measured data of the roughness of the meteorite fragments was only at the submicrometer scale, and it is not known whether roughness features at scales larger than the submicrometer scale can be extrapolated to the scale of the fine-grained matrix for chondrite particles that did not experience planetary differentiation and, to some extent, retained the primary texture of the mineral assemblage (*23*).

If we neglect the effect of the grain shape, based on the measured cohesive force of silica spheres proportional to the reduced particle radius (*13*), the typical grain radius, or asperity radius, of the

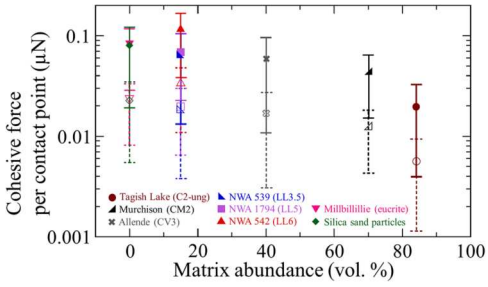

Fig. 2. Cohesive forces of meteorite fragments and abundance of matrix in the meteorites. Open symbols and dashed error bars indicate measurements under ambient conditions. The Tagish Lake and Allende meteorite values were obtained in this study; all other values are based on a previous study (*14*). The cohesive force per contact point between particles was corrected by one-half [because values obtained using the centrifugal method were measured between a particle and a slide (*10*–*13*)] and one-third (because particles of tens of micrometers in size were in contact with a slide at approximately three points, as shown in Fig. 1, B to D). Matrix abundance values were obtained from previous studies (*23*, *53*). Plots and error bars represent typical values and the range of the cumulative number fraction corresponding to 0.25 to 0.75, calculated by fitting Eq. 3 to the measurements, respectively. Closed symbols and solid error bars represent cohesive forces 3.5-fold greater than those measured under ambient conditions (see Materials and Methods). The values are summarized in Table 1.

particle surfaces $\overline{R_{\mathrm{asp}}}$ can be calculated from the typical cohesive force $\overline{F_{\mathrm{meas}}}$ measured under ambient conditions with a high probability of three-point contact for particles that are tens of micrometers in size (table S5), based on $(\overline{F_{\mathrm{meas}}}/3)/\overline{R_{\mathrm{asp}}} = 0.18$ N/m. In Table 1, we summarize the values of $\overline{R_{\mathrm{asp}}}$, which ranged from 0.06 to 0.4 μm. The typical sizes of silicate matrix grains found in the carbonaceous chondrites ALHA 77307 (CO3.0), QUE 99177 (CR2), MIL07687 (unclassified), and Acfer 094 (unclassified) are 0.1 to 0.2 μm (*24*). The size range of the majority of individual grains in chondritic porous interplanetary dust particles is ~0.050 to 0.2 μm (*25*). The $\overline{R_{\mathrm{asp}}}$ and sizes of these grains were comparable. However, the fragments for which cohesive force measurements were conducted in this study included components other than the matrix.

The cohesive force of particles on the surface of asteroids has conventionally been estimated on the basis of the van der Waals force for spheres, which is proportional to the particle size, and the Hamaker constant of lunar regolith particles (*2*, *3*). Alternatively, on the basis of the values of ordinary chondrite and carbonaceous chondrite fragments after heating in Table 1, we assume that the cohesive forces per contact point between S- and C-type asteroid particles are 0.02 to 0.06 μN and 0.07 to 0.1 μN, respectively, and are independent of fragment size as long as plastic deformation does not occur.

The number of contact points between particles depends on the ratio between the gravitational and cohesive forces or the Bond number (*2*, *4*). Micrometer- and tens-of-micrometer–sized particles deposited under the Earth's gravity contact the slide at approximately one and three points, respectively (Fig. 1, B to D), suggesting that the millimeter scale is the lower particle size limit at which three-point contact occurs on subkilometer-sized bodies (see Materials and Methods). We considered the total cohesive force of the particles on the bodies to be three times the cohesive force per contact point. However, particles larger than tens of centimeters in diameter may deform plastically under their weight, and their cohesive force may increase with weight.

Compared to the previous assumption that the cohesive force is proportional to the particle size (*3*), the total cohesive force per fragment proposed in this study is of smaller magnitude orders (Fig. 3A), suggesting that particles on a small body are much more mobile than previously expected when subjected to perturbing forces (e.g., due to seismic wave accelerations by impacts). When we evaluated the mobility of particles on a small body in terms of the pressure (e.g., of gasses) required to overcome gravity and the cohesive force [(*3*); see Materials and Methods], the calculated pressure based on the cohesive force proposed in this study was minimal for particles as small as 1 cm, which was also lower than previously expected (Fig. 3B). Evidence of mass transfer has been found on the asteroids Itokawa, Ryugu, and Bennu (*26*–*28*). Spacecraft contact with the surface of Bennu revealed near-zero interparticle cohesion (*29*, *30*). The size of particles covering the lower areas of Itokawa (*26*), ejected from Bennu (*31*), and ejected during sample collection and rover hops on Ryugu (*32*) ranged from the millimeter to centimeter scale, from <1 to 10 cm, and the centimeter size, respectively. The estimates determined in this study were consistent with these observations.

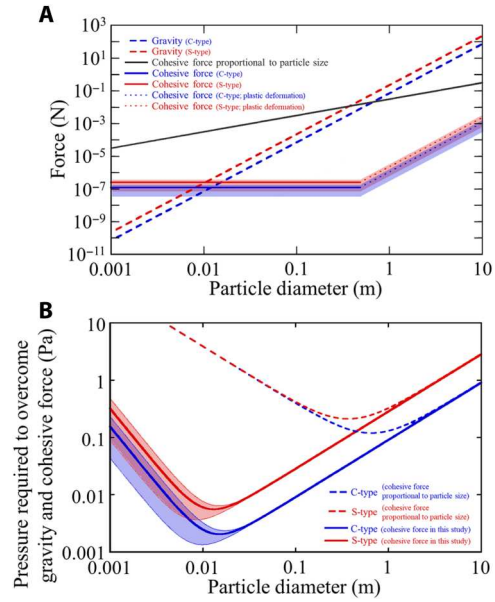

Fig. 3. Low cohesive force and high surface mobility of asteroid particles. (**A**) Comparison of gravity and cohesive forces acting on particles on the surfaces of C- and S-type asteroids with a diameter of 0.5 km. Dashed lines indicate gravity. Gray solid line indicates a cohesive force proportional to particle size. Blue and red solid lines indicate threefold those of typical cohesive forces per contact point listed in Table 1. We assumed that typical cohesive forces for C- and S-type asteroids were the averages for carbonaceous and ordinary chondrites, respectively. Filled areas represent the predicted range of the cohesive force for particles with averaged typical cohesive forces. The range of the cohesive force corresponding to a cumulative number fraction of 0.25 to 0.75 was approximately 0.28 to 1.5 times the typical cohesive force on average (Table 1). Dotted lines indicate the predicted cohesive forces, considering plastic deformation due to the particle's weight. (**B**) Pressure required to overcome gravity and cohesive force [(*3*), Eq. 9]. Dashed curves indicate the case of the cohesive force proportional to the particle size. Solid curves indicate the case of the cohesive force obtained in this study (see Materials and Methods).

Table 1. $\overline{R_{asp}}$ and cohesive force per contact point for meteorite fragments after heating.

		Asperity	Cohesive force	
		$\overline{R_{asp}}$ (μm)	Typical (μN)	Range (μN)
Carbonaceous chondrites	Tagish Lake	0.063	0.020	0.0039–0.033
	Murchison*	0.14	0.044	0.015–0.064
	Allende	0.19	0.059	0.011–0.096
Ordinary chondrites	NWA 539*	0.21	0.065	0.013–0.10
	NWA 1794*	0.22	0.069	0.023–0.11
	NWA 542*	0.38	0.12	0.038–0.17
Achondrite	Millbillillie*	0.26	0.082	0.029–0.12

*On the basis of the measurements of a previous study (*14*).

MATERIALS AND METHODS

Preparation of particles

We examined two carbonaceous chondrite samples from Tagish Lake (C2-ung) and Allende (CV3). We prepared micrometer-sized and tens-of-micrometer–sized meteorite fragments. The former was prepared only for the Allende meteorite. The meteorite pieces were crushed using an agate mortar and pestle. We used sieves to eliminate particles >75 and <25 μm in size for the tens-of-micrometer–sized samples, and >16 and <5 μm in size for the micrometer-sized samples (hereinafter referred to as "small"). We also collected samples of ejecta fragments arising from projectile impact on the pieces. Low-velocity (0.129 to 0.136 km s^{-1}) impact experiments were conducted at ambient pressure using a helium gas gun installed at Kobe University and $^1/_8$-inch stainless steel spherical projectiles. High-velocity (2.85 to 2.92 km s^{-1}) impact experiments were conducted at reduced pressure (a few pascals) using a two-stage hydrogen gas gun at the Institute of Space and Astronautical Science and 1-mm aluminum spherical projectiles. The experimental conditions are listed in table S1. Ejecta fragments were recovered in acrylic containers. The fragment size was limited to 25 to 75 μm and prepared using the same procedure as that applied for the ground particles. The SEM images of the sample surfaces are shown in fig. S1. The Tagish Lake samples had much finer surface structures than the Allende samples, whether crushed by mortar and pestle or by impact.

For a sample with a known surface structure, we used aggregates of polydisperse silica spheres (Admatechs Co. Ltd.) with a density of 2.26 g cm^{-3} (manufacturer's information). The cumulative number fraction of the diameters of the 186 spheres measured in the SEM images is shown in fig. S2. The diameters were in the range of 0.1 to 1 μm, with a median of 0.44 μm. It is possible to prepare aggregates of mesh size or smaller by sieving them (*33*, *34*). We prepared aggregates using a sieve with a mesh size of 106 μm and selected aggregates tens of micrometers in size for the measurements.

The cumulative number fraction of the equivalent circular diameter of the samples measured from the optical microscope images is shown in fig. S2. The Tagish Lake and Allende have grain densities of 2.72 and 3.56 g cm^{-3}, respectively (*14*, *35*), and the bulk porosities of their hand-sized samples are 40 and 22% on average, respectively (*35*, *36*). We used the grain density literature value for each meteorite as its upper fragment density limit. We assumed a bulk density of 0.84 g cm^{-3} for the aggregates according to the previously reported average filling factor for silica sphere aggregates from the submillimeter to millimeter scale (*33*, *34*). The median equivalent circular diameters and densities of the samples are presented in table S2.

Shape of particles

We obtained the axial ratio and circularity of the samples to characterize and compare the shape of fragments using the optical microscope images with a spatial resolution of 1.3 or 0.66 μm $pixel^{-1}$ using ImageJ software (*37*) in experiments different from those of cohesive-force measurements. We obtained the axial ratio ($A_x = b/a$), that is, the length ratio of the minor axis b to the major axis a when the two-dimensional (2D) projection of the particle is approximated as an ellipse. We also obtained circularity ($C = 4\pi S/L^2$), where S is the projection area and L is its perimeter. Because circularity depends on the spatial resolution of the image (*14*), it was based on measurements obtained at a spatial resolution where the 2D projected area of the particle corresponded to 10^3 to 5×10^3 pixels. Table S3 presents the average, SD, and median values of the axial ratio and circularity of the particles. The axial ratios of the meteorite fragments, including the ejecta fragments, ranged from 0.71 to 0.75, similar to the b/a ratios of meteorite fragments reported in a previous study as well as basalt impact fragments, Itokawa particles, and Itokawa, Eros, and Ryugu boulders (*14*). The axis ratio of the aggregates was slightly higher, with an average value of 0.79. The circularity of meteorite fragments and aggregates ranged from 0.73 to 0.78. These circularity values are similar to those of fine basalt impact fragments (*14*).

We obtained the surface morphologies of one or two particles from each sample using a confocal laser scanning microscope (LEXT OLS3100) with horizontal and vertical resolutions of 0.125 and 0.01 μm, respectively. We also obtained the values for the smooth glass slide used to measure the cohesive force. The surface morphologies of the particles obtained from each sample are shown in fig. S3A. We randomly extracted two to three line scans from each surface profile and calculated the arithmetic mean roughness (R_a) for each scan of 20-μm length, as described in a previous study (*14*). The samples of the line scans are shown in fig. S3B. The line scans of an Allende ground fragment and silica sand particle of similar size (*14*) are also shown for comparison. The R_a value of the glass slide was 3 nm. The surface asperity of the stainless steel slide is on the order of a few nanometers (manufacturer's information). The silica spheres constituting the aggregates were too small to be assessed for roughness using the confocal laser microscope; however, the surface appeared smooth even in the SEM image (~4 nm per pixel, fig. S1). The R_a values of the meteorite fragments and aggregates were at the submicrometer scale, whereas those of the silica sand particles were on the order of tens of nanometers (*14*). The silica sand particles and slides differed in R_a by orders of magnitude, and the differences

among meteorites and aggregates were not substantial. The mean R_a values and SDs are listed in table S4.

Heating of particles

We measured the cohesive force after the samples were heated to remove any water molecules absorbed on the particle surfaces under ambient conditions. Because meteorites can be altered by heating, we conducted simultaneous thermal analysis using a thermogravimetry/differential thermal analyzer (TG-DTA) (Rigaku Thermo plus EVO). The Allende and Tagish Lake samples (13.9 and 15.7 mg, respectively) were placed in a platinum container, with an empty container used as a reference, and the containers were heated simultaneously in dry air at a rate of 5°C min^{-1} to 300°C and then at a rate of 10°C min^{-1} to 600°C. By simultaneously measuring the change in the sample mass and temperature difference from the reference (to detect an exothermic or endothermic reaction), we checked for the presence or absence of a material change at each temperature. On the basis of these results, we determined the heating temperature required to remove adsorbed water molecules from the Allende and Tagish Lake samples while avoiding alteration.

The weight change rates of the Allende and Tagish Lake samples measured using TG-DTA are shown in fig. S4. As the temperature increased, the Allende sample began to lose mass; it reached a minimum at 200° to 300°C and then began to gain mass and generate heat above 400°C. The initial loss of mass was attributed to the removal of adsorbed water molecules; the total mass lost was 0.02 mg, which corresponds to a volume of ~0.027 cm^3 for water molecules assuming an ideal gas at 1 atm and 25°C. Thus, a volume of 2 cm^3 was lost per gram, which is similar to the amount of water vapor adsorbed in the previous study (*14*). The subsequent increase in mass may have been caused by sample oxidation, as observed during heating of the lunar regolith (*38*). In contrast, the Tagish Lake sample exhibited an endothermic reaction at approximately 60°C and lost several 10-fold more mass than the Allende sample before reaching 300°C. At temperatures above 400°C, the sample begins to lose more mass in an endothermic reaction. The former loss of mass may have included the removal of adsorbed water molecules and dehydration of interlayer water, as observed during the heating of saponite (*39*). The latter loss of mass may have corresponded to hydroxyl release from layer silicates and CO_2 release from carbonates at ≥400°C (*39*). To avoid the effects of oxidation and thermal decomposition, we set the heating of the meteorite fragments for cohesive force measurements to temperatures below 400°C, i.e., 120°, 250°, and 330°C. However, interlayer water dehydration can occur in Tagish Lake samples at ≥60°C. The DTA signals changed when the heating rate was switched at 300°C, which might indicate irreversible changes in the samples. However, a previous study of DTA of Allende meteorite at a heating rate of 80°C min^{-1} showed no signal change at ~300°C (*40*). We did not conduct TG-DTA for aggregates consisting of silica spheres but heated them at 330°C for 24 hours for cohesive-force measurements, thereby matching the duration, and with an even higher temperature than in a previous study that investigated the effect of adsorbed water molecules on the tensile strength of aggregates consisting of silica spheres (*16*).

Cohesive-force measurements of particles

In this study, we measured the cohesive force between a particle and circular optical glass (20 mm in diameter) and a polished circular stainless steel plate of 8 mm in diameter (slides) using a centrifugal method (*14*, *19*, *20*). This method allowed us to directly and simultaneously measure the cohesive forces of irregularly shaped particles to obtain statistical data.

All measurements started with particles deposited on the slide in open air at 25 to 50% relative humidity. We observed that deposition while using an ionizer to reduce the effects of electrostatic charging did not substantially affect the results. For some samples, the particles were subsequently evacuated (~10 or 10^{-3} Pa) or heated. The heating conditions were determined, as described in the previous section. A schematic of the cohesive force measurement configuration for reduced pressure is shown in fig. S5. The volume enclosed by the valved mini-vacuum chamber and glass slide was evacuated at room or elevated temperatures. The valve was closed, and vacuum was maintained during the cohesive force measurement. Heating was performed using a hot plate, as shown in fig. S5. As we could not measure the heating temperature along with the cohesive force owing to space limitations on the glass slide and in the mini-vacuum chamber, we conducted a calibration experiment. We measured the temperature of the glass slide surface without placing the fragments. The slide attached to the chamber was heated on the hot plate, and the temperature was measured using a digital thermometer based on a K thermocouple sensor. The equilibrium temperatures on the slide reached approximately 120°, 250°, and 330°C within a few tens of minutes after switching on the heater at different settings. As shown in table S5, the heating duration including the rise time was 1, 24, or 48 hours.

Optical microscopy images of the particles on the slide were acquired, as shown in fig. S5. Next, we placed the slide in a centrifuge and applied centrifugal force to it in the direction in which the particles were pulled off vertically. The slide was then gently removed from the centrifuge tube. Optical microscope images were taken at the same location after centrifugal force was applied (fig. S5). We replaced the slide in the centrifuge and applied greater centrifugal force. The procedure was repeated as the centrifugal acceleration β of the particles was increased from 1×10^1 to 3×10^3 g_E (g_E is the acceleration of the Earth's gravity) in 7 to 10 steps using a tabletop centrifuge (Kubota KN-70). For evacuated or heated measurements, we placed a pair of mini-vacuum chambers with valves in the centrifuge and captured microscope images from outside the chamber using a mini-vacuum chamber jig developed for this study (fig. S5). For small particles (micrometer scale), we used a floor-standing micro-ultracentrifuge (himac CS150FNX) to apply β of 1×10^3 to 6×10^5 g_E to the particles. We used only stainless steel slides because large accelerations can fragment glass slides.

If a particle is small and its gravity is small compared with the cohesive force, the particle may stick unsteadily when it comes into contact with a slide. Therefore, we pressed particles onto a slide using centrifugal force prior to the cohesive force measurements (*20*) and measured the cohesive force after pressing small Allende fragments against a stainless steel slide under a centrifugal acceleration of approximately 8×10^4 g_E.

The mass M of each particle used to calculate the centrifugal force was estimated using the a-axis length of each particle, as measured in the optical microscope images, and the particle density ρ_P

(table S2), as follows

$$M = \varphi_v \rho_p a^3 \quad (1)$$

where ϕ_v is a shape-dependent coefficient. The previously obtained average ϕ_v values were 0.12 and 0.08 for meteorite fragments (average axial ratio $A_x = 0.72$) and glass particles (average $A_x = 0.58$), respectively (*14*). Using the two data points and $(A_x, \phi_v) = (1, \pi/6)$, we derive the following empirical relationship

$$\varphi_v = \frac{\pi}{6} e^{(-4.76 \pm 0.32)(1 - A_x)} \quad (2)$$

We assumed that $\phi_v = 0.19$ for aggregates, with $A_x = 0.79$ on average. There was approximately 40% uncertainty in ϕ_v, considering the uncertainty in the axial ratio, up to a few tens of percent uncertainty in ρ_p for meteorite fragments depending on whether it is close to the grain density or the bulk density of meteorite, and a 14 to 15% uncertainty in ρ_p for aggregates (*33*, *34*); thus, an uncertainty of up to approximately 50% in the single-particle mass was expected.

As reported in a previous study (*14*), the cohesive force between a particle and slide was determined as $M\sqrt{\beta_i \beta_{i+1}}$, where β_i is the maximum centrifugal acceleration at which the particle remains on the slide and β_{i+1} is the centrifugal acceleration at which the particle no longer remains on the slide. Owing to the uncertainty in the particle mass and acceleration derived from the geometric mean of the two values, 50% or more uncertainty in the single-particle cohesive force was expected. In this study, we measured the cohesive force of at least 88% of the particles in each sample type. Table S5 summarizes the number and measured number fraction of the particles.

Measured cohesive force under heated and evacuated conditions

Figure S6 shows the cumulative number fractions f of the measured cohesive force, F_{meas}, against a glass slide under various conditions for the Allende, Tagish Lake, and aggregate samples. Cohesive force data were plotted starting at 10^{-3} μN at intervals of $\sqrt{5}$ and fitted with the following equation (*14*)

$$f_{F_{meas}}(< F_{meas}) = 1 - \exp\left\{-\left(\frac{F_{meas} - F_{meas0}}{\overline{F_{meas}}}\right)^{\psi_{F_{meas}}}\right\} \quad (3)$$

where $\overline{F_{meas}}$ is a typical value of F_{meas}, $\psi_{F_{meas}}$ is a parameter characterizing the width of the distribution, and F_{meas0} is a threshold parameter set to the minimum value of the measurements. Table S5 summarizes the values of each parameter. The cohesive force was affected by heating before the measurements, although no clear dependence on heating temperature or duration was observed. The measured cohesive force of the Allende fragments and aggregates after heating was approximately three- to fourfold larger for $\overline{F_{meas}}$ than at ambient temperature. This was consistent with the two- to threefold increase in cohesion observed in direct shear tests for sand and silica under heating and evacuating conditions (*41*–*43*) and the ≤7-fold increase in the surface energy of silica obtained by the unified measurement method in previous studies (*15*). However, the increase was smaller than the previously estimated ≤10-fold increase in surface energy based on the tensile strength measurements of aggregates consisting of silica spheres (*16*). The larger increase reported in previous studies may be attributable to the uncertainty of the relationship between the tensile strength and cohesive force.

The measured cohesive force of the Tagish Lake meteorite fragments was also approximately three- to fourfold larger after heating than at ambient temperature. To explore the possibility that the removal of interlayer water at these temperatures affects the cohesive force of the Tagish Lake fragments, we conducted two additional heating measurements. The first was performed on Tagish Lake fragments that were heated at 250°C for 1 hour, cooled to ambient temperature in ambient air, and then deposited on a glass slide. The second measurement was performed after the fragments used in the first measurement were reheated to 250°C for 1 hour. As shown in fig. S6, in the former experiment, the measured cohesive force was not significantly different from that obtained without heating (Mann-Whitney U test, $P = 0.13$). This may be because the surface chemistry of the slide and fragments was reset. In the latter experiment, the measured cohesive force was increased. Therefore, even if the interlayer water was lost due to heating, cohesive force was not substantially affected. Table 1 summarizes the 3.5-fold cohesive force under ambient conditions, that is, the values obtained after heating.

Plastic deformation of particles

If we assume Hertzian contact mechanics (*44*), when two elastic bodies in contact with each other had surface asperity radii R_{asp1} and R_{asp2}, Young's moduli E_1 and E_2, and Poisson's ratios ν_1 and ν_2 were compressed against each other by a force F, the resulting maximum contact pressure P_{max} was as follows

$$P_{max} = \left(\frac{6FE^{*2}}{\pi^3 R_{asp}{}^2}\right)^{1/3} \quad (4)$$

$$\frac{1}{E^*} = \frac{1 - \nu_1{}^2}{E_1} + \frac{1 - \nu_2{}^2}{E_2} \quad (5)$$

$$\frac{1}{R_{asp}} = \frac{1}{R_{asp1}} + \frac{1}{R_{asp2}} \quad (6)$$

where we assume that R_{asp1} is 0.2 μm for small Allende fragments with an a-axis length of 6 μm. We assume only one point of contact with the slide. We used 73 GPa and 0.17 [vitreous silica: (*45*)] as the Young's modulus and Poisson's ratio, respectively, for the fragments, and 191 GPa and 0.3 [stainless steel: (*46*)], respectively, as those for the slide. Substituting $F = M\beta$, where M is one particle mass (Eq. 1), the P_{max} of the small Allende fragments pressed on the stainless steel slide at $\beta = 8 \times 10^4\ g_E$ is estimated to be ~1 GPa. Because it does not exceed the theoretical strength of silica glass of 24 GPa (*47*), the increase in cohesive force due to pressing for small Allende fragments is due to the increase in contact points rather than plastic deformation. Furthermore, we observed that the cohesive force of Murchison meteorite fragments tens of micrometers in size, measured under ambient conditions, remained largely unchanged regardless of whether they were pressed against a glass slide at $\beta = 5 \times 10^3\ g_E$. If they had a contact area similar to that of the Allende fragments, they would have been subjected to greater pressure than the small Allende fragments; however, the cohesive

force did not change, suggesting that plastic deformation was absent.

Cohesive force of particles on small bodies

A previous study assumed a van der Waals force between two macroscopic spheres to be the cohesive force (*3*). Figure 3A shows the van der Waals force (*10*)

$$F_{\mathrm{VDW}} = \frac{A}{12t^2}\frac{d_{\mathrm{p}}}{2} \tag{7}$$

and gravity if we ignore the effect of the asteroid's rotation for simplicity

$$F_{\mathrm{g}} = \frac{\pi\rho_{\mathrm{p}}{d_{\mathrm{p}}}^3}{6}\left(\frac{4\pi G\rho_{\mathrm{a}}}{3}\right)\frac{d_{\mathrm{a}}}{2} \tag{8}$$

acting on a spherical particle with diameter d_{p} on spherical C-type and S-type asteroids with diameters d_{a} = 0.5 km. We assume the Hamaker constant was $A = 6.5 \times 10^{-20}$ J, the distance between particle surfaces was $t = 3 \times 10^{-10}$ m for glass (*48*), and a single contact point between particles. In the equation, G is the gravitational constant, ρ_{a} is the bulk density of the asteroid, and ρ_{p} is the bulk density of the particle. We assumed that the ρ_{a} values of the C- and S-type asteroids were 1190 kg m^{-3} (*30*, *49*) and 1900 kg m^{-3} (*50*), respectively, and that the ρ_{p} values of the C- and S-type asteroid particles were 1640 kg m^{-3} [Tagish Lake: (*35*)] and 3220 kg m^{-3} [average for LL chondrites: (*51*)], respectively. Figure 3A also shows our proposed cohesive forces of particles on small bodies, using the values listed in Table 1. The surface chemistry of the particles may be affected by space weathering processes and is not well known (*52*); however, even if the cohesive force is greater than that we proposed, the increase is likely to be at most an order of magnitude, given the range of measured surface energies under various conditions (*15*). As shown in Fig. 3B, when a particle on the surface is subjected to pressure, such as gas pressure, in the cross-sectional area, the pressure p required for the particle to overcome gravity F_{g} and cohesive force F_{c} and thus become separated from the surface can be written as in a previous study (*3*) as follows

$$p = \frac{F_{\mathrm{g}} + F_{\mathrm{c}}}{\pi\left(\frac{d_{\mathrm{p}}}{2}\right)^2} \tag{9}$$

From the results shown in Fig. 1B, it is likely that, under Earth's gravity, ~60-μm Allende meteorite fragments and aggregates were in contact with the slides at roughly three points, and ~6-μm Allende meteorite fragments were in contact with the slide at one point. The median masses of these particles were approximately 1×10^{-10}, 0.6×10^{-10}, and 1×10^{-13} kg, respectively, with the Bond number $B_{\mathrm{o}} = F_{\mathrm{c}}/F_{\mathrm{g}}$ calculated as approximately 0.03, 0.01, and 2×10^{-5}, respectively, assuming F_{c} is $1/3\overline{F_{\mathrm{meas}}}$ for the ~60-μm particles and $\overline{F_{\mathrm{meas}}}$ for the ~6-μm particles, respectively. This result suggests that a value of B_{o} greater than 0.01 would result in approximately three contact points on the surface, whereas a value of B_{o} less than 2×10^{-5} would result in a single contact point. The former situation corresponds to particles ≥1 mm in size on subkilometer-sized asteroids, using the cohesive force listed in Table 1.

The plastic deformation of the particles can lead to a greater cohesive force. We considered the possibility of plastic deformation on asteroids using the typical radius of the surface asperity $\overline{R_{\mathrm{asp}}}$ in Table 1. Assuming for simplicity that $R_{\mathrm{asp1}} = R_{\mathrm{asp2}} \approx 0.2$ μm and $F = \pi/6\rho_{\mathrm{p}}d^3g$, where d is the particle diameter, g is the gravitational acceleration on the surface of an asteroid, and particles are held on the surface at N contact points, Eq. 4 can be rewritten as follows

$$P_{\max} \sim \frac{15}{N}\left(\frac{d}{10\ \mathrm{cm}}\right)\left(\frac{\rho_{\mathrm{p}}}{2500\ \mathrm{kgm}^{-3}}\right)^{1/3}\left(\frac{g}{10^{-4}\ \mathrm{ms}^{-2}}\right)^{1/3}\ \mathrm{GPa} \tag{10}$$

where Young's modulus and Poisson's ratio of the particles were assumed to be 73 GPa and 0.17, respectively [vitreous silica: (*45*)]. This result suggests that the gravitational pressure on particles smaller than several tens of centimeters on the surface of a 0.5-km–sized asteroid does not exceed the theoretical strength of silica glass (24 GPa) (*47*). However, plastic deformation may occur in larger particles. We assume that the particles break up, increasing the number of contact points (N), which reduces $P_{\max}$; in this case, N may increase in proportion to the applied force F. Thus, the cohesive force may increase in proportion to F. This hypothesis is supported by a previous study, which showed that the measured cohesive force of particles increases linearly with the preliminary applied force owing to plastic deformation (*20*). Thus, Fig. 3A also shows that the cohesive force is assumed to be proportional to the third power of particle sizes above ~48 cm, which is the diameter at which $N = 3$ and $P_{\max} = 24$ GPa.

Supplementary Materials

This PDF file includes:

Figs. S1 to S6
Tables S1 to S5
Legends data S1 to S4

Other Supplementary Material for this manuscript includes the following:

Data S1 to S4

REFERENCES AND NOTES

1. S. J. Weidenschilling, Dust to planetesimals: Settling and coagulation in the solar nebula. *Icarus* **44**, 172–189 (1980).
2. D. J. Scheeres, C. M. Hartzell, P. Sánchez, M. Swift, Scaling forces to asteroid surfaces: The role of cohesion. *Icarus* **210**, 968–984 (2010).
3. E. B. Bierhaus, J. T. Songer, B. C. Clark, R. D. Dubisher, S. L. Deden, K. S. Payne, D. Wurts, J. W. McMahon, B. Rozitis, D. S. Lauretta, Bennu regolith mobilized by TAGSAM: Expectations for the OSIRIS-REx sample collection event and application to understanding naturally ejected particles. *Icarus* **355**, 114142 (2021).
4. M. Kiuchi, A. M. Nakamura, Relationship between regolith particle size and porosity on small bodies. *Icarus* **239**, 291–293 (2014); Corrigendum to "Relationship between regolith particle size and porosity on small bodies". *Icarus* **248**, 221–221 (2015).
5. C. M. Schäfer, S. Scherrer, R. Buchwald, T. I. Maindl, R. Speith, W. Kley, Numerical simulations of regolith sampling processes. *Planet. Space Sci.* **141**, 35–44 (2017).
6. M. Hirabayashi, D. P. Sánchez, D. J. Scheeres, Internal structure of asteroids having surface shedding due to rotational instability. *Astrophys. J.* **808**, 63 (2015).
7. K. Sugiura, H. Kobayashi, S. I. Watanabe, H. Genda, R. Hyodo, S. I. Inutsuka, SPH simulations for shape deformation of rubble-pile asteroids through spinup: The challenge for making top-shaped asteroids Ryugu and Bennu. *Icarus* **365**, 114505 (2021).

8. J. D. Iversen, J. B. Pollack, R. Greeley, B. R. White, Saltation threshold on Mars: The effect of interparticle force, surface roughness, and low atmospheric density. *Icarus* **29**, 381–393 (1976).
9. Y. Shao, H. Lu, A simple expression for wind erosion threshold friction velocity. *J. Geophys. Res. Atmos.* **105**, 22437–22443 (2000).
10. J. N. Israelachvili, *Intermolecular and Surface Forces* (Elsevier Academic Press, 2015).
11. K. L. Johnson, K. Kendall, A. Roberts, Surface energy and the contact of elastic solids. *Proc. R. Soc. Lond. A Math. Phys. Sci.* **324**, 301–313 (1971).
12. B. V. Derjaguin, V. M. Muller, Y. P. Toporov, Effect of contact deformations on the adhesion of particles. *J. Colloid Interface Sci.* **53**, 314–326 (1975).
13. L. O. Heim, J. Blum, M. Preuss, H. J. Butt, Adhesion and friction forces between spherical micrometer-sized particles. *Phys. Rev. Lett.* **83**, 3328–3331 (1999).
14. Y. Nagaashi, T. Aoki, A. M. Nakamura, Cohesion of regolith: Measurements of meteorite powders. *Icarus* **360**, 114357 (2021).
15. H. Kimura, K. Wada, H. Senshu, H. Kobayashi, Cohesion of amorphous silica spheres: Toward a better understanding of the coagulation growth of silicate dust aggregates. *Astrophys. J.* **812**, 67 (2015).
16. T. Steinpilz, J. Teiser, G. Wurm, Sticking properties of silicates in planetesimal formation revisited. *Astrophys. J.* **874**, 60 (2019).
17. K. R. Housen, L. L. Wilkening, C. R. Chapman, R. Greenberg, Asteroidal regoliths. *Icarus* **39**, 317–351 (1979).
18. M. Delbo, G. Libourel, J. Wilkerson, N. Murdoch, P. Michel, K. T. Ramesh, C. Ganino, C. Verati, S. Marchi, Thermal fatigue as the origin of regolith on small asteroids. *Nature* **508**, 233–236 (2014).
19. Y. Nagaashi, T. Omura, M. Kiuchi, A. M. Nakamura, K. Wada, S. Hasegawa, Laboratory experiments on agglomeration of particles in a granular stream. *Prog. Earth Planet Sci.* **5**, 52 (2018). doi:10.1186/s40645-018-0205-6. Erratum: Correction to: Laboratory experiments on agglomeration of particles in a granular stream. *Prog. Earth Planet Sci.* **5**, 71 (2018). doi:10.1186/s40645-018-0233-2.
20. K. K. Lam, J. M. Newton, Investigation of applied compression on the adhesion of powders to a substrate surface. *Powder Technol.* **65**, 167–175 (1991).
21. L. T. Zhuravlev, The surface chemistry of amorphous silica. Zhuravlev model. *Colloids Surf. A. Physicochem. Eng. Asp.* **173**, 1–38 (2000).
22. B. N. J. Persson, J. Biele, On the stability of spinning asteroids. *Tribol. Lett.* **70**, 34 (2022).
23. M. K. Weisberg, T. J. McCoy, A. N. Krot, Systematics and evaluation of meteorite classification, in *Meteorites and the Early Solar System II*, D. S. Lauretta, H. Y. McSween Jr., Eds. (University of Arizona Press, 2006), pp. 19–52.
24. E. Vaccaro, "Physical and chemical properties of matrix in primitive chondrites," thesis, The Open University, United Kingdom (2017).
25. P. J. Wozniakiewicz, J. P. Bradley, H. A. Ishii, M. C. Price, D. E. Brownlee, Pre-accretional sorting of grains in the outer solar nebula. *Astrophys. J.* **779**, 164 (2013).
26. H. Miyamoto, H. Yano, D. J. Scheeres, S. Abe, O. Barnouin-Jha, A. F. Cheng, H. Demura, R. W. Gaskell, N. Hirata, M. Ishiguro, T. Michikami, A. M. Nakamura, R. Nakamura, J. Saito, S. Sasaki, Regolith migration and sorting on asteroid Itokawa. *Science* **316**, 1011–1014 (2007).
27. S. Sugita, R. Honda, T. Morota, S. Kameda, H. Sawada, E. Tatsumi, M. Yamada, C. Honda, Y. Yokota, T. Kouyama, N. Sakatani, K. Ogawa, H. Suzuki, T. Okada, N. Namiki, S. Tanaka, Y. Iijima, K. Yoshioka, M. Hayakawa, Y. Cho, M. Matsuoka, N. Hirata, N. Hirata, H. Miyamoto, D. Domingue, M. Hirabayashi, T. Nakamura, T. Hiroi, T. Michikami, P. Michel, R.-L. Ballouz, O. S. Barnouin, C. M. Ernst, S. E. Schröder, H. Kikuchi, R. Hemmi, G. Komatsu, T. Fukuhara, M. Taguchi, T. Arai, H. Senshu, H. Demura, Y. Ogawa, Y. Shimaki, T. Sekiguchi, T. G. Müller, A. Hagermann, T. Mizuno, H. Noda, K. Matsumoto, R. Yamada, Y. Ishihara, H. Ikeda, H. Araki, K. Yamamoto, S. Abe, F. Yoshida, A. Higuchi, S. Sasaki, S. Oshigami, S. Tsuruta, K. Asari, S. Tazawa, M. Shizugami, J. Kimura, T. Otsubo, H. Yabuta, S. Hasegawa, M. Ishiguro, S. Tachibana, E. Palmer, R. Gaskell, L. Le Corre, R. Jaumann, K. Otto, N. Schmitz, P. A. Abell, M. A. Barucci, M. E. Zolensky, F. Vilas, F. Thuillet, C. Sugimoto, N. Takaki, Y. Suzuki, H. Kamiyoshihara, M. Okada, K. Nagata, M. Fujimoto, M. Yoshikawa, Y. Yamamoto, K. Shirai, R. Noguchi, N. Ogawa, F. Terui, S. Kikuchi, T. Yamaguchi, Y. Oki, Y. Takao, H. Takeuchi, G. Ono, Y. Mimasu, K. Yoshikawa, T. Takahashi, Y. Takei, A. Fujii, C. Hirose, S. Nakazawa, S. Hosoda, O. Mori, T. Shimada, S. Soldini, T. Iwata, M. Abe, H. Yano, R. Tsukizaki, M. Ozaki, K. Nishiyama, T. Saiki, S. Watanabe, Y. Tsuda, The geomorphology, color, and thermal properties of Ryugu: Implications for parent-body processes. *Science* **364**, 252 (2019).
28. K. J. Walsh, E. R. Jawin, R.-L. Ballouz, O. S. Barnouin, E. B. Bierhaus, H. C. Connolly Jr., J. L. Molaro, T. J. McCoy, M. Delbo', C. M. Hartzell, M. Pajola, S. R. Schwartz, D. Trang, E. Asphaug, K. J. Becker, C. B. Beddingfield, C. A. Bennett, W. F. Bottke, K. N. Burke, B. C. Clark, M. G. Daly, D. N. DellaGiustina, J. P. Dworkin, C. M. Elder, D. R. Golish, A. R. Hildebrand, R. Malhotra, J. Marshall, P. Michel, M. C. Nolan, M. E. Perry, B. Rizk, A. Ryan, S. A. Sandford, D. J. Scheeres, H. C. M. Susorney, F. Thuillet, D. S. Lauretta; The OSIRIS-REx Team, Craters, boulders and regolith of (101955) Bennu indicative of an old and dynamic surface. *Nat. Geosci.* **12**, 242–246 (2019).
29. D. S. Lauretta, C. D. Adam, A. J. Allen, R.-L. Ballouz, O. S. Barnouin, K. J. Becker, T. Becker, C. A. Bennett, E. B. Bierhaus, B. J. Bos, R. D. Burns, H. Campins, Y. Cho, P. R. Christensen, E. C. A. Church, B. E. Clark, H. C. Connolly Jr., M. G. Daly, D. N. Dellagiustina, C. Y. D. d'Aubigny, J. P. Emery, H. L. Enos, S. F. Kasper, J. B. Garvin, K. Getzandanner, D. R. Golish, V. E. Hamilton, C. W. Hergenrother, H. H. Kaplan, L. P. Keller, E. J. Lessac-Chenen, A. J. Liounis, H. Ma, L. K. Mccarthy, B. D. Miller, M. C. Moreau, T. Morota, D. S. Nelson, J. O. Nolau, R. Olds, M. Pajola, J. Y. Pelgrift, A. T. Polit, M. A. Ravine, D. C. Reuter, B. Rizk, B. Rozitis, A. J. Ryan, E. M. Sahr, N. Sakatani, J. A. Seabrook, S. H. Selznick, M. A. Skeen, A. A. Simon, S. Sugita, K. J. Walsh, M. M. Westermann, C. W. V. Wolner, K. Yumoto, Spacecraft sample collection and subsurface excavation of asteroid (101955) Bennu. *Science* **377**, 285–291 (2022).
30. K. J. Walsh, R.-L. Ballouz, E. R. Jawin, C. Avdellidou, O. S. Barnouin, C. A. Bennett, E. B. Bierhaus, B. J. Bos, S. Cambioni, H. C. Connolly Jr., M. Delbo, D. N. Dellagiustina, J. Demartini, J. P. Emery, D. R. Golish, P. C. Haas, C. W. Hergenrother, H. Ma, P. Michel, M. C. Nolan, R. Olds, B. Rozitis, D. C. Richardson, B. Rizk, A. J. Ryan, P. Sánchez, D. J. Scheeres, S. R. Schwartz, S. H. Selznick, Y. Zhang, D. S. Lauretta, Near-zero cohesion and loose packing of Bennu's near subsurface revealed by spacecraft contact. *Sci. Adv.* **8**, eabm6229 (2022).
31. D. S. Lauretta, C. W. Hergenrother, S. R. Chesley, J. M. Leonard, J. Y. Pelgrift, C. D. Adam, M. Al Asad, P. G. Antreasian, R.-L. Ballouz, K. J. Becker, C. A. Bennett, B. J. Bos, W. F. Bottke, M. Brozović, H. Campins, H. C. Connolly Jr., M. G. Daly, A. B. Davis, J. De León, D. N. Dellagiustina, C. Y. D. d'Aubigny, J. P. Dworkin, J. P. Emery, D. Farnocchia, D. P. Glavin, D. R. Golish, C. M. Hartzell, R. A. Jacobson, E. R. Jawin, P. Jenniskens, J. N. Kidd Jr., E. J. Lessac-Chenen, J.-Y. Li, G. Libourel, J. Licandro, A. J. Liounis, C. K. Maleszewski, C. Manzoni, B. May, L. K. Mccarthy, J. W. Mcmahon, P. Michel, J. L. Molaro, M. C. Moreau, D. S. Nelson, W. M. Owen Jr., B. Rizk, H. L. Roper, B. Rozitis, E. M. Sahr, D. J. Scheeres, J. A. Seabrook, S. H. Selznick, Y. Takahashi, F. Thuillet, P. Tricarico, D. Vokrouhlický, C. W. V. Wolner, Episodes of particle ejection from the surface of the active asteroid (101955) Bennu. *Science* **366**, eaay3544 (2019).
32. S. Tachibana, H. Sawada, R. Okazaki, Y. Takano, K. Sakamoto, Y. N. Miura, C. Okamoto, H. Yano, S. Yamanouchi, P. Michel, Y. Zhang, S. Schwartz, F. Thuillet, H. Yurimoto, T. Nakamura, T. Noguchi, H. Yabuta, H. Naraoka, A. Tsuchiyama, N. Imae, K. Kurosawa, A. M. Nakamura, K. Ogawa, S. Sugita, T. Morota, R. Honda, S. Kameda, E. Tatsumi, Y. Cho, K. Yoshioka, Y. Yokota, M. Hayakawa, M. Matsuoka, N. Sakatani, M. Yamada, T. Kouyama, H. Suzuki, C. Honda, T. Yoshimitsu, T. Kubota, H. Demura, T. Yada, M. Nishimura, K. Yogata, A. Nakato, M. Yoshitake, A. I. Suzuki, S. Furuya, K. Hatakeda, A. Miyazaki, K. Kumagai, T. Okada, M. Abe, T. Usui, T. R. Ireland, M. Fujimoto, T. Yamada, M. Arakawa, H. C. Connolly Jr., A. Fujii, S. Hasegawa, N. Hirata, N. Hirata, C. Hirose, S. Hosoda, Y. Iijima, H. Ikeda, M. Ishiguro, Y. Ishihara, T. Iwata, S. Kikuchi, K. Kitazato, D. S. Lauretta, G. Libourel, B. Marty, K. Matsumoto, T. Michikami, Y. Mimasu, A. Miura, O. Mori, K. Nakamura-Messenger, N. Namiki, A. N. Nguyen, L. R. Nittler, H. Noda, R. Noguchi, N. Ogawa, G. Ono, M. Ozaki, H. Senshu, T. Shimada, Y. Shimaki, K. Shirai, S. Soldini, T. Takahashi, Y. Takei, H. Takeuchi, R. Tsukizaki, K. Wada, Y. Yamamoto, K. Yoshikawa, K. Yumoto, M. E. Zolensky, S. Nakazawa, F. Terui, S. Tanaka, T. Saiki, M. Yoshikawa, S. Watanabe, Y. Tsuda, Pebbles and sand on asteroid (162173) Ryugu: In situ observation and particles returned to Earth. *Science* **375**, 1011–1016 (2022).
33. R. Weidling, C. Güttler, J. Blum, Free collisions in a microgravity many-particle experiment. I. Dust aggregate sticking at low velocities. *Icarus* **218**, 688–700 (2012).
34. S. Kothe, J. Blum, R. Weidling, C. Güttler, Free collisions in a microgravity many-particle experiment. III. The collision behavior of sub-millimeter-sized dust aggregates. *Icarus* **225**, 75–85 (2013).
35. A. R. Hildebrand, P. J. A. McCausland, P. G. Brown, F. J. Longstaffe, S. D. J. Russell, E. Tagliaferri, J. F. Wacker, M. J. Mazur, The fall and recovery of the Tagish Lake meteorite. *Meteorit. Planet. Sci.* **41**, 407–431 (2006).
36. R. J. Macke, G. J. Consolmagno, D. T. Britt, Density, porosity, and magnetic susceptibility of carbonaceous chondrites. *Meteorit. Planet. Sci.* **46**, 1842–1862 (2011).
37. C. A. Schneider, W. S. Rasband, K. W. Eliceiri, NIH Image to ImageJ: 25 years of image analysis. *Nat. Methods* **9**, 671–675 (2012).
38. A. Dąbrowski, E. Mendyk, E. Robens, K. Skrzypiec, J. Goworek, M. Iwan, Z. Rzączyńska, Investigation of surface properties of lunar regolith part III. *J. Therm. Anal. Calorim.* **94**, 633–639 (2008).
39. C. M. Gilmour, C. D. Herd, P. Beck, Water abundance in the Tagish Lake meteorite from TGA and IR spectroscopy: Evaluation of aqueous alteration. *Meteorit. Planet. Sci.* **54**, 1951–1972 (2019).
40. P. G. Simmonds, A. J. Bauman, E. M. Bollin, E. Gelpi, J. Oró, The unextractable organic fraction of the Pueblito de Allende meteorite: Evidence for its indigenous nature. *Proc. Natl. Acad. Sci. U.S.A.* **64**, 1027–1034 (1969).
41. E. Vey, J. D. Nelson, Engineering properties of simulated lunar soils. *J. Soil Mech. Found. Div.* **91**, 25–52 (1965).

42. L. G. Bromwell, "The friction of quartz in high vacuum" (Massachusetts Institute of Technology Research Report R66-18, 1966).
43. J. D. Nelson, E. Vey, Relative cleanliness as a measure of lunar soil strength. *J. Geophys. Res.* **73**, 3747–3764 (1968).
44. H. Hertz, Miscellaneous papers (Macmillan 146, 1896).
45. S. Spinner, Temperature dependence of elastic constants of vitreous silica. *J. Am. Ceram. Soc.* **45**, 394–397 (1962).
46. J. Xie, Z. Zhu, T. Yang, M. Dong, R. Li, The effect of incident angle on the rebound behavior of micro-particle impacts. *J. Aerosol Sci.* **155**, 105778 (2021).
47. I. Naray-Szabo, J. Ladik, Strength of silica glass. *Nature* **188**, 226–227 (1960).
48. S. Alvo, P. Lambert, M. Gauthier, S. Régnier, A van der Waals force-based adhesion model for micromanipulation. *J. Adhes. Sci. Technol.* **24**, 2415–2428 (2010).
49. S. Watanabe, M. Hirabayashi, N. Hirata, N. A. Hirata, R. Noguchi, Y. Shimaki, H. Ikeda, E. Tatsumi, M. Yoshikawa, S. Kikuchi, H. Yabuta, T. Nakamura, S. Tachibana, Y. Ishihara, T. Morota, K. Kitazato, N. Sakatani, K. Matsumoto, K. Wada, H. Senshu, C. Honda, T. Michikami, H. Takeuchi, T. Kouyama, R. Honda, S. Kameda, T. Fuse, H. Miyamoto, G. Komatsu, S. Sugita, T. Okada, N. Namiki, M. Arakawa, M. Ishiguro, M. Abe, R. Gaskell, E. Palmer, O. S. Barnouin, P. Michel, A. S. French, J. W. Mcmahon, D. J. Scheeres, P. A. Abell, Y. Yamamoto, S. Tanaka, K. Shirai, M. Matsuoka, M. Yamada, Y. Yokota, H. Suzuki, K. Yoshioka, Y. Cho, S. Tanaka, N. Nishikawa, T. Sugiyama, H. Kikuchi, R. Hemmi, T. Yamaguchi, N. Ogawa, G. Ono, Y. Mimasu, K. Yoshikawa, T. Takahashi, Y. Takei, A. Fujii, C. Hirose, T. Iwata, M. Hayakawa, S. Hosoda, O. Mori, H. Sawada, T. Shimada, S. Soldini, H. Yano, R. Tsukizaki, M. Ozaki, Y. Iijima, K. Ogawa, M. Fujimoto, T.-M. Ho, A. Moussi, R. Jaumann, J.-P. Bibring, C. Krause, F. Terui, T. Saiki, S. Nakazawa, Y. Tsuda, Hayabusa2 arrives at the carbonaceous asteroid 162173 Ryugu—A spinning top-shaped rubble pile. *Science* **364**, 268–272 (2019).
50. A. Fujiwara, J. Kawaguchi, D. K. Yeomans, M. Abe, T. Mukai, T. Okada, J. Saito, H. Yano, M. Yoshikawa, D. J. Scheeres, O. Barnouin-Jha, A. F. Cheng, H. Demura, R. W. Gaskell, N. Hirata, H. Ikeda, T. Kominato, H. Miyamoto, A. M. Nakamura, R. Nakamura, S. Sasaki, K. Uesugi, The rubble-pile asteroid Itokawa as observed by Hayabusa. *Science* **312**, 1330–1334 (2006).
51. G. J. Consolmagno, D. T. Britt, R. J. Macke, The significance of meteorite density and porosity. *Geochemistry* **68**, 1–29 (2008).
52. Y. Igami, S. Muto, A. Takigawa, M. Ohtsuka, A. Miyake, K. Suzuki, K. Yasuda, A. Tsuchiyama, Structural and chemical modifications of oxides and OH generation by space weathering: Electron microscopic/spectroscopic study of hydrogen-ion-irradiated Al_2O_3. *Geochim. Cosmochim. Acta* **315**, 61–72 (2021).
53. A. Takayama, K. Tomeoka, Fine-grained rims surrounding chondrules in the Tagish Lake carbonaceous chondrite: Verification of their formation through parent-body processes. *Geochim. Cosmochim. Acta* **98**, 1–18 (2012).

Acknowledgments: We thank Y. Seto (Osaka Metropolitan University) for the technical assistance regarding the preparation of the cohesive force measurement system in a vacuum environment. We thank A. Matsuoka (Kobe University) for the technical assistance provided for simultaneous TG-DTA. This research was supported by the Hypervelocity Impact Facility (formerly the Space Plasma Laboratory), ISAS, JAXA. **Funding:** This work was supported by the Sasakawa Scientific Research Grant from The Japan Science Society (to Y.N.) and JSPS KAKENHI grant 21H00044 (to A.M.N.). **Author contributions:** Conceptualization: Y.N. and A.M.N. Methodology: Y.N. and A.M.N. Investigation: Y.N. Visualization: Y.N. Project administration: A.M.N. Supervision: A.M.N. Writing—original draft: Y.N. Writing—review and editing: A.M.N. **Competing interests:** The authors declare that they have no competing interests. **Data and materials availability:** All data needed to evaluate the conclusions in the paper are present in the paper and/or the Supplementary Materials.

Submitted 6 June 2022
Accepted 10 February 2023
Published 17 March 2023
10.1126/sciadv.add3530